Molecular ion-pair states in ungerade H_2

Adam Kirrander[1] and Christian Jungen[1,2]

[1]*Laboratoire Aimé Cotton du Centre National de la Recherche Scientifique, Université de Paris–Sud, F-91405 Orsay, France*

[2]*Department of Physics and Astronomy, University College London, Gower Street, London WC1E 6BT, United Kingdom*

(Received 11 October 2011; published 18 November 2011)

Molecular ion-pair states are analogs of electronic Rydberg states, but with the electron replaced by a much heavier ion. We calculate *ab initio* the long-range vibrational H^+H^- ion-pair states in H_2 for ungerade $^1\Sigma_u^+$ symmetry, corresponding to recent observations by Ekey and McCormack [Phys. Rev. A **84**, 020501 (2011)]. The overall trends in the experiment are reproduced and many peaks can be assigned. The calculations yield interloper resonances corresponding to vibrational states trapped inside the barriers on the potential-energy curves $5,6\,^1\Sigma_u^+$.

DOI: 10.1103/PhysRevA.84.052512 PACS number(s): 33.20.Wr, 32.80.Ee, 33.80.Gj

I. INTRODUCTION

Rydberg states, characterized by long-range Coulomb interactions, are normally associated with states consisting of an electron and a positively charged atomic or molecular ion, but can also occur as vibrational states in ionic bonds between atoms. Compared to normal vibrational states these have unusual properties, including extremely large internuclear distances and, in principle, an infinity of states below the ion-pair dissociation limit. In general, molecular ion-pair states can participate in the dissociative photodynamics of a wide range of molecules and are exploited in threshold ion-pair product spectroscopy [1] to provide precise measurements of positive ions otherwise difficult to study [2].

The ion-pair (*heavy* Rydberg) states can decay via nonadiabatic couplings that lead to electron transfer and subsequent dissociation into neutral atoms. In the specific case of H_2, it has been suggested that mutual neutralization of H^+H^- may affect the astrophysically important H_2 formation rate [3,4], although the abundance of H^- in space is debated [5]. In addition, in many molecules the ion-pair states are embedded in the electronic Rydberg continuum with complicated coupling to ionization.

A remarkable opportunity to unravel the dynamics of ion-pair states comes from a series of recent energy-resolved experiments. In the experiments, spectra of vibrational ion-pair states have been observed in photoexcited H_2, by Vieitez *et al.* in the $^1\Sigma_g^+$ symmetry [6,7] and more recently in the $^1\Sigma_u^+$ symmetry by Ekey and McCormack [8], while Mollet and Merkt observed ion-pair states with quantum numbers beyond 1500 in Cl_2 [9].

In this paper we provide an analysis of the experimental spectra [8] of the ungerade H_2 ion-pair states, bound by the outer well of potential-energy curve $6\,^1\Sigma_u^+$. The observed heavy Rydberg series is strongly perturbed; however, the characteristic pattern in the resonance positions is reproduced (see Fig. 4), including even some of the perturbations, by a theory that does not take account of the coupling to ionization and the Rydberg continuum. We find that nonadiabatic couplings and interloper resonances play a stronger role than in the gerade $^1\Sigma_g^+$ symmetry [10], especially for vibrational states with a bias toward smaller internuclear distances. A tentative assignment of interloper resonances is made (see Table I).

The theory is essentially contained in Ref. [10]. We calculate the ion-pair states, positions, and widths from first principles using *ab initio* potential-energy curves and nonadiabatic couplings [11,12]. The close-coupled equations for nuclear motion [13] are solved by the log-derivative method [14]. The main approximation is the exclusion of the ionization and the electronic Rydberg continua and of the nonhomogenous coupling to $^1\Pi_u$ electronic states. These effects become important at small internuclear distances, approximately for $R < 5$ a.u.

II. THEORY

The ion-pair states are bound by the long-range Coulomb potential (in a.u.) [15]

$$E^{\rm ion}(R) = D_{\rm H^+H^-} - \frac{1}{R} - \frac{\alpha_{\rm H^-}}{2R^4}, \tag{1}$$

where $D_{\rm H^+H^-} = -0.527\,751\,014$ a.u. [16] is the ion-pair dissociation energy and the polarizability of $H^-(1s^2)$ is $\alpha_{\rm H^-} = 211.897$ (a.u.)^3 [17]. The energy levels in the Coulomb potential are given by the Rydberg formula

$$E_n = D_{\rm H^+H^-} - \frac{[2hc\,{\rm Ry}_\infty](M/m_e)}{2[n_{\rm IP} - \mu(E)]^2}, \tag{2}$$

where $n_{\rm IP}$ is the principal quantum number and $\mu(E)$ is the quantum defect. The quantity in square brackets $[2hc\,{\rm Ry}_\infty]$ corresponds to 1 a.u. of energy. Furthermore, $\rm Ry_\infty$ is the infinite-mass Rydberg constant, $M/m_e = 918.5761$ is the mass-scaling factor with M the reduced mass of H^- and m_e the mass of an electron. The quantum defect μ gives the shift in the position of each Rydberg level compared to a pure unperturbed Coulomb potential. The shifts are caused by short-range interactions and, to some extent, by the long-range polarizability of the ion-pair potential. For high enough principal quantum numbers $n_{\rm IP}$, the quantum defect becomes independent of energy. In heavy Rydberg systems, such as H^+H^-, this occurs for much higher $n_{\rm IP}$ than in a typical electronic Rydberg system [10]. This relates to the fact that the classical outer turning point $R_{\rm tp}$ for a Rydberg state is approximately

$$R_{\rm tp} \approx \frac{2n_{\rm IP}^2}{M/m_e} \tag{3}$$

in atomic units. Consequently, for a given $n_{\rm IP}$, Rydberg states with $M/m_e \gg 1$ are more compact and have a larger part of the wave function in the short-range interaction region.

We solve the close-coupled equations for nonadiabatic nuclear motion [13]

$$\left(-\frac{1}{2M_{H_2}}\left[\mathbf{1}\frac{d^2}{dR^2} - \mathbf{1}\frac{J(J+1)}{R^2} + \boldsymbol{A}(R) + \boldsymbol{B}(R)\frac{d}{dR}\right] + \boldsymbol{U}(R) - \mathbf{1}E\right)\tilde{\Psi}(R) = 0, \quad (4)$$

where the value of the reduced mass for H_2 is $M_{H_2} \approx 918.0764$ [11], $\boldsymbol{U}(R)$ contains the N' clamped-nuclei electronic energy curves, E is the total energy, and $\boldsymbol{A}(R)$ and $\boldsymbol{B}(R)$ are the $N' \times N'$ nonadiabatic coupling matrices. The required data are obtained from Refs. [11,12]. The first-derivative coupling term can be eliminated by a Cayley transform

$$\left[\mathbf{1}\frac{d}{dR} + \boldsymbol{B}(R)\right]\boldsymbol{C}(R) = 0, \quad (5)$$

with the boundary condition $\boldsymbol{C}(R \to \infty) = \mathbf{1}$. The matrix $\boldsymbol{C}(R)$ defines the adiabatic-diabatic transformation. This allows us to transform Eq. (4) to the standard form

$$\boldsymbol{\Psi}''(R) = \boldsymbol{W}(R)\boldsymbol{\Psi}(R), \quad (6)$$

where $\boldsymbol{\Psi}$ is an $N' \times N'$ matrix, each column is a linearly independent solution, $\boldsymbol{\Psi}''$ indicates the second derivative with respect to R, and the matrix $\boldsymbol{W}$ consists of

$$\boldsymbol{W}(R) = \frac{2M}{\hbar^2}\boldsymbol{V}(R) - \boldsymbol{k}^2, \quad (7)$$

where the $N' \times N'$ matrix $\boldsymbol{V}$ contains the diagonal potentials (including the angular momentum components) and the off-diagonal coupling elements. The diagonal matrix $\boldsymbol{k}$ contains the asymptotic channel wave vectors $\boldsymbol{k}^2 = (2M/\hbar^2)\boldsymbol{\epsilon}$, where $\boldsymbol{\epsilon}$ has diagonal elements $\epsilon_i = E - E_i$, with E the total energy and E_i the threshold energy in each channel i.

Equation (6) is solved using the log-derivative method [14,18], which propagates the log-derivative matrix $\boldsymbol{Y}(R) = \boldsymbol{\Psi}'(R)\boldsymbol{\Psi}^{-1}(R)$ instead of propagating the wave function $\boldsymbol{\Psi}$ directly. This avoids numerical stability problems in classically forbidden regions. The matrix is propagated out to the matching radius R_f, where it is used to calculate the wave function in the form $\boldsymbol{\Psi} = \boldsymbol{F} - \boldsymbol{G}\boldsymbol{K}$, where $\boldsymbol{F}$ and $\boldsymbol{G}$ are diagonal $N \times N$ matrices containing energy normalized Milne functions [19]. These coincide with analytic Coulomb and Riccati-Bessel functions once the polarization term in Eq. (1) vanishes. Note that $N \leqslant N'$ since channels closed already at R_f are excluded from $\boldsymbol{\Psi}$. The crucial entity is the $N \times N$ reaction matrix $\boldsymbol{K}$, which summarizes all interactions for $R < R_f$. From the scattering matrix, we can calculate the cumulative eigenphase for the half-collision scattering and the energy derivative of the eigenphase gives the density of states. The peaks in the density of states allow us to determine the position of each resonance and hence the quantum defect via Eq. (2). The predissociation width is obtained from the full width at half maximum for each peak.

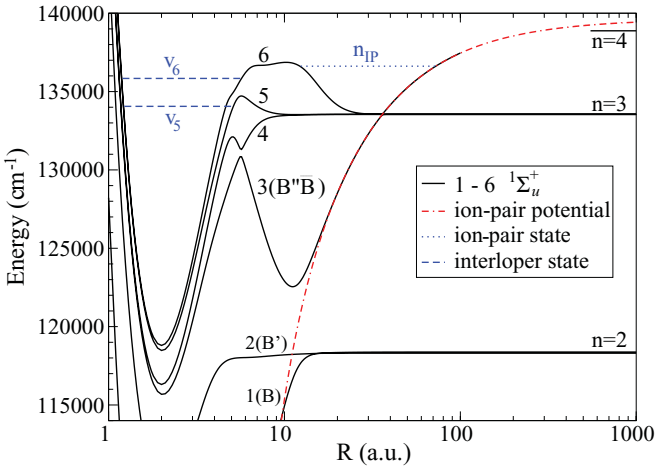

FIG. 1. (Color online) Adiabatic *ab initio* potential-energy curves 1–6 $^1\Sigma_u^+$ for H_2 [11], with the energy in cm^{-1} relative to the $X\,^1\Sigma_g^+(v = 0, J = 0)$ ground state. The analytic ion-pair potential is included [see Eq. (1)] and open dissociation channels correspond to H($n = 1$) + H($n = 2,3$). The closed $n = 4$ dissociation level is also indicated. Interloper resonances trapped inside the barriers on potential-energy curves 5,6 $^1\Sigma_u^+$ are indicated by horizontal lines and are labeled with quantum numbers v_5 and v_6, respectively. The ion-pair outer-well states on 6 $^1\Sigma_u^+$ are labeled by the principal quantum number $n_{\rm IP}$ [see Eq. (2)]. Note that Staszewska and Wolniewicz [11] use quantum numbers v_3, v_1, and v_2 rather than v_5, v_6, and $n_{\rm IP}$.

III. CALCULATION

Figure 1 shows the adiabatic *ab initio* potential-energy curves for the $^1\Sigma_u^+$ symmetry of H_2 calculated by Staszewska and Wolniewicz [11]. The ion-pair states are bound by the Coulomb potential given in Eq. (1), which is included in Fig. 1. Between the dissociation limits $n = 3$ and 4, the energy region currently of interest, the Coulomb potential matches the external part of the outer well on the potential-energy curve 6 $^1\Sigma_u^+$. The open dissociation channels correspond to H($n = 1$) + H($n = 2,3$). The nonadiabatic couplings are taken from Wolniewicz, Orlikowski, and Staszewska [12]. The couplings are strongest for $R < 20$ a.u., but extend to $R = 80$ a.u. Since the present calculations concern states with $n_{\rm IP} \leqslant 215$, with relatively small classical turning points $R_{\rm tp} \leqslant 100$ a.u., we do not use the long-range channel elimination procedure outlined in Ref. [10].

We solve the nonadiabatic equations for the nuclear motion for energies 133 640–137 400 cm^{-1} and total angular momentum $J = 0$–2. In the experiment [8] the $J = 2$ series should be dominant. The calculated density of states is shown in Fig. 2. The range of resonances corresponds to states with principal quantum numbers $n_{\rm IP} = 130$–215. The first states to appear with amplitude in the outer well on the potential-energy curve 6 $^1\Sigma_u^+$ are 133 641.50 cm^{-1} ($n_{\rm IP} = 129.55$), 133 640.93 cm^{-1} ($n_{\rm IP} = 129.54$), and 133 640.01 cm^{-1} ($n_{\rm IP} = 129.53$) for $J = 0$, 1, and 2, respectively. Note that for most other resonances in the outer well, the $J = 0$ peaks appear at the lowest energies and the $J = 2$ peaks at the highest. The three calculated $J = 0$–2 ion-pair series are very similar. The exceptions are the inside-the-barrier interlopers indicated in Fig. 1 and shown in detail in Fig. 3. The short-range character

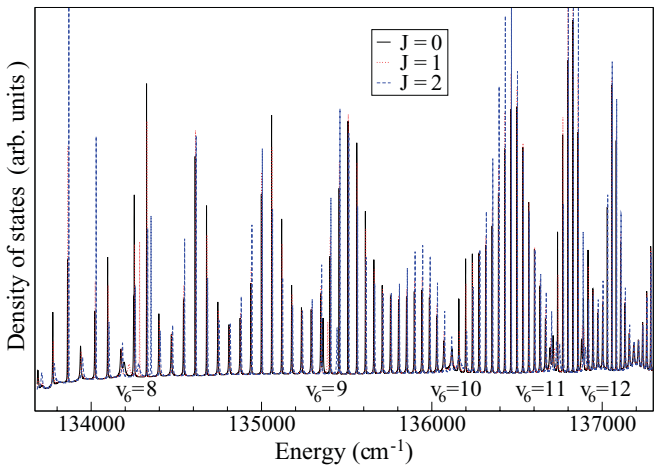

FIG. 2. (Color online) Calculated resonances (density of states) for $H_2\ ^1\Sigma_u^+$ with $J = 0,1,2$ plotted as a function of the energy in cm^{-1} relative the H_2 ground state. The progression of ion-pair states, almost identical for the three J series, is perturbed by the presence of interloper resonances. The regions where the interlopers are found are labeled by the quantum number v_6 and are shown in detail in Fig. 3. The density of states is calculated from the derivative of the cumulative eigenphase $d\left(\sum_\rho \pi\tau_\rho(E)\right)/dE$.

of the interlopers make them sensitive to the value of J (see the large shifts between interlopers with different J in Fig. 3). They can be assigned quantum numbers $v_6 = 8$–12 and $v_5 = 9$ by comparison to adiabatic (predissociated) levels calculated on the single potential-energy curves $6\ ^1\Sigma_u^+$ and $5\ ^1\Sigma_u^+$, respectively. Although no state is uniquely associated with $v_6 = 10$, this interloper perturbs the surrounding ion-pair states, as can be seen in the quantum defects in Fig. 4. The

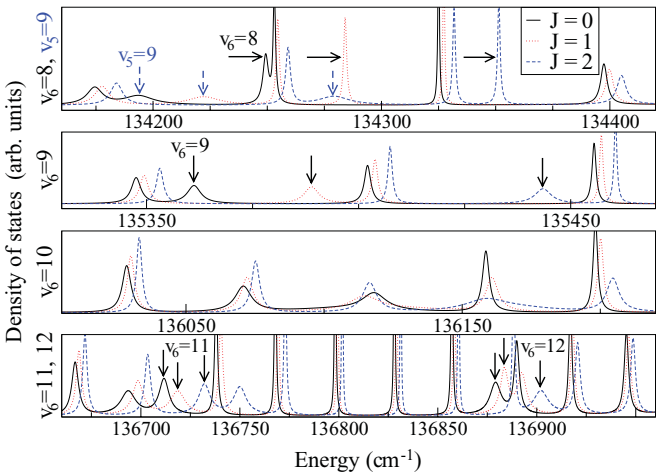

FIG. 3. (Color online) Resonances from Fig. 2 in the regions perturbed by interloper resonances. Most of the interlopers (indicated by solid black arrows) originate from the $6\ ^1\Sigma_u^+$ potential-energy curve, with inner-well quantum numbers $v_6 = 8$–12, although the states corresponding to $v_6 = 10$ are strongly mixed with the ion-pair resonances in the same region. The $v_5 = 9$ interlopers (indicated by vertical dashed arrows in the top panel) on $5\ ^1\Sigma_u^+$ occur in the same region as $v_6 = 8$. Unlabeled resonances correspond to outer-well (ion-pair) states. All resonances appear in sets of 3, corresponding to $J = 0$, 1, and 2.

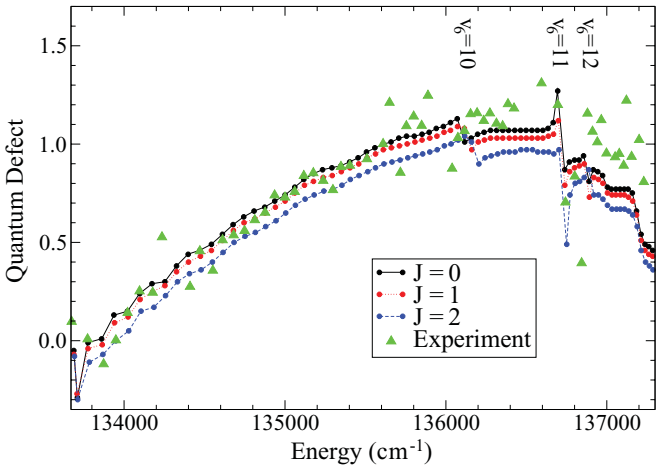

FIG. 4. (Color online) Comparison between calculated quantum defects for $J = 0$–2 ion-pair states and quantum defects from experimental term values [20] for the experiment in Ref. [8]. The actual quantum defects for the interloper resonances are not included. Initially, the quantum defects increase, similarly to what was observed in $^1\Sigma_g^+$ [10], but for energies greater than 136 000 cm^{-1} they go flat and then drop dramatically. The interlopers $v_6 = 10 - 12$ leave an imprint on the quantum defects by perturbing the progression of ion-pair states, despite the fact that the $v_6 = 10$ resonances do not appear as unique states and are strongly mixed with the ion-pair states in the same region (see Fig. 3).

$v_5 = 9$ assignment is confirmed by a nonadiabatic calculation without the $5\ ^1\Sigma_u^+$ potential, in which the surrounding peaks remain essentially unaffected while the peak assigned to $v_5 = 9$ disappears. In adiabatic calculations $v_5 = 10$ resonances appear for $J = 0$ and 1, but these are absent when the full set of coupled equations is solved. Interloper states with $v_5 < 9$ and $v_6 < 8$ are below the $n = 3$ dissociation limit.

IV. RESULTS

Figure 4 compares the calculated quantum defects with those corresponding to the experimental observations [20]. The quantum defects, defined by Eq. (2), give the deviation of the actual ion-pair levels relative to an ideal Rydberg series. As can be seen in Fig. 4, the calculations reproduce the main trends in the experiment. The quantum defects show a strong energy dependence. For less than 136 000 cm^{-1} ($n_{IP} < 170$) the quantum defects increase with energy in similar fashion to the quantum defects calculated for the $^1\Sigma_g^+$ symmetry, but then, essentially between $v_6 = 10$ and 11, the $^1\Sigma_u^+$ quantum defects go flat and for greater than 136 000 cm^{-1} ($n_{IP} > 185$) there is a sharp drop. The smooth increase in the quantum defects for less than 136 000 cm^{-1} is associated with the short-range dynamics on the $B''\bar{B}$ potential-energy curve, but at higher energies no simple interpretation is possible. The strong energy dependence of the quantum defects is not surprising given that the series consists of low-n_{IP} members of the heavy Rydberg states, which have H^+H^- character only during a small part of the dynamics. Accounting for the mass scaling implied by Eqs. (2) and (3), typical Rydberg behavior is not expected until $n_{IP} \geqslant 500$ [10].

TABLE I. Positions and assignments of interlopers (see the text and Figs. 1–3). The energies labeled E_{calc} correspond to resonance positions obtained from the full nonadiabatic calculations, while E_{adiab} corresponds to adiabatic energies on $6\,^1\Sigma_u^+$ (quantum number v_6) or on $5\,^1\Sigma_u^+$ (quantum number v_5). States are assigned by vibrational quantum number and total angular momentum J. For $J = 2$, we match the calculated levels with the closest experimental level E_{expt} [20]. The state $v_6 = 10$ is strongly mixed with the ion-pair resonances (see the text and Fig. 3). Energies are given in cm^{-1}.

E_{calc}	E_{adiab}	Assignment	E_{expt}
134193.52	134164.3	$v_5 = 9, J = 0$	
134222.16	134193.4	$v_5 = 9, J = 1$	
134279.16	134251.1	$v_5 = 9, J = 2$	134290.0
134249.32	134242.3	$v_6 = 8, J = 0$	
134284.12	134276.7	$v_6 = 8, J = 1$	
134351.43	134344.1	$v_6 = 8, J = 2$	134371.0
135361.21	135345.2	$v_6 = 9, J = 0$	
135388.88	135372.9	$v_6 = 9, J = 1$	
135443.49	135426.6	$v_6 = 9, J = 2$	135446.5
	136060.3	$v_6 = 10, J = 0$	
	136081.4	$v_6 = 10, J = 1$	
	136122.3	$v_6 = 10, J = 2$	
136711.68	136673.1	$v_6 = 11, J = 0$	
136718.61	136689.6	$v_6 = 11, J = 1$	
136732.11	136720.3	$v_6 = 11, J = 2$	136729.0
136879.21	136872.0	$v_6 = 12, J = 0$	
136883.66	136879.9	$v_6 = 12, J = 1$	
136902.08	136892.3	$v_6 = 12, J = 2$	

The average fit between the calculated $J = 2$ ion-pair resonances and all 72 levels observed in experiment is 7 cm^{-1}. Although this is not perfect, the energy range over which this fit is valid and the large number of states (quantum numbers range from $n_{IP} = 130$ to 211) make the identification of the ion-pair heavy Rydberg series convincing. The overall agreement with the experimental quantum defects is also good, but clearly the experimental spectra have substantial structure not captured by the present dissociation-only calculations.

Although the quantum defects corresponding to the interloper states are not explicitly shown in Fig. 4, the $v_6 = 10$–12 interlopers leave a distinct perturbation in the quantum defects. In Table I, which lists nonadiabatic and adiabatic energy levels, an attempt is made to associate calculated interlopers for $J = 2$ with experimental levels by listing the closest experimental level [20] that has not already been assigned to the ion-pair Rydberg series. The agreement is not very good, especially for $v_5 = 9$ and $v_6 = 8$, but the $v_6 = 9$ and 11 assignments are more believable with $\Delta E \approx 3$ cm^{-1}. The assignments are particularly interesting because they are a first step towards bridging the gap between observations in the inner and outer wells of molecular hydrogen.

The widths of the resonances are not reported in the experiment [8], but we are able to calculate them. The widths, shown in Fig. 5, vary across the energy range and the interloper resonances are *broader*, i.e., more dissociated, than the ion-pair widths. This is in direct contrast to what was found in the $^1\Sigma_g^+$ symmetry [10], where the resonances were monotonically decreasing in width and interlopers were sharper than ion-pair resonances.

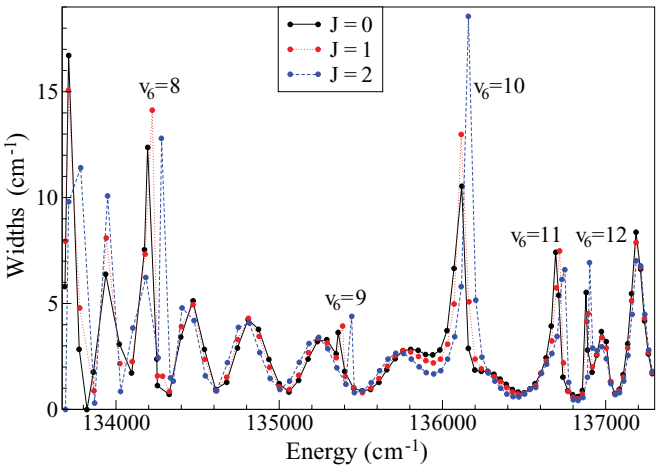

FIG. 5. (Color online) Linewidths in cm^{-1} for the calculated resonances in Fig. 2 with $J = 0,1,2$, obtained as the full width at half maximum for each resonance peak. Compared to previous calculations in $^1\Sigma_g^+$ [10], there is a significant modulation of the linewidths and the interloper resonances (some of them labeled) are wider than the ion-pair states instead of sharper.

The oscillations in the linewidths are similar to the oscillations in the photodissociation cross section observed in the $B''\bar{B}\,^1\Sigma_u^+$ potential at lower energies [21,22]. There the oscillations could be attributed to the strong adiabatic correction lifting the barrier separating the inner and outer wells on the $B''\bar{B}$ electronic state, periodically localizing the wave

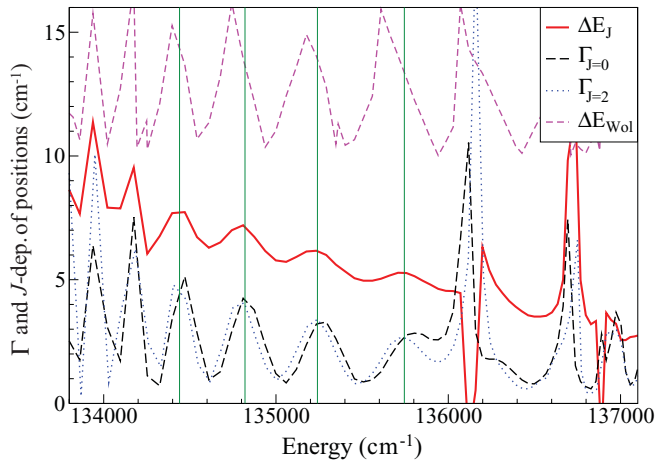

FIG. 6. (Color online) Linewidths and nonadiabatic effects correlate with the localization of the wave function at small or large internuclear distances as measured by ΔE_J, which is calculated as the difference between the ion-pair resonance positions for $J = 2$ and 0. The linewidths Γ (shown for $J = 0$ and 2, with interloper resonances excluded) are largest when ΔE_J is large and hence when the wave functions skewed toward *small* internuclear distances. The curve labeled ΔE_{Wol} shows the effect of the nonadiabatic couplings on level positions by calculating the difference between the positions of our nonadiabatic resonances and the adiabatic (single potential-energy curve) bound levels calculated by Staszewska and Wolniewicz [11]. The ΔE_{Wol} curve has been multiplied by 0.2 and shifted by $+10$ cm^{-1}. Overall, the levels are most strongly shifted when the wave function is skewed toward small internuclear distances. The units are cm^{-1} throughout.

function at shorter distances. Although the present experiment is above this barrier, we can nonetheless correlate the observed modulation to the structure of the wave functions by calculating the difference ΔE_J between the positions of the $J = 2$ and 0 ion-pair resonances. The value ΔE_J gives an indication of whether the wave function is skewed toward small (ΔE_J large) or large (ΔE_J small) internuclear distances. This is because the $J(J+1)/R^2$ term in the Hamiltonian exerts a stronger shift on short-range states. In Fig. 6, ΔE_J is shown together with the $\Gamma_{J=0,2}$ widths (excluding interlopers) and the difference ΔE_{Wol} between the adiabatic outer-well levels calculated by Staszewska and Wolniewicz [11] and the level positions for the full nonadiabatic calculations. Clearly, the variation in ΔE_J correlates with both the widths $\Gamma_{J=0,2}$ and the error in the adiabatic calculations ΔE_{Wol}. This indicates that the wave functions with a bias towards short internuclear distances are most affected by nonadiabatic couplings and are more predissociated. Similar conclusions regarding the widths of resonances can be drawn in the context of autoionization [23].

V. CONCLUSION

Our nonadiabatic *ab initio* calculations reproduce the main characteristics of recent spectra (see Fig. 4) of ungerade $^1\Sigma_u^+$ heavy Rydberg ion-pair series in molecular hydrogen [8]. A tentative assignment (see Table I) of two inside-the-barrier interloper resonances is made; these were predicted also in the gerade $^1\Sigma_g^+$ spectrum [10], but no experimental levels corresponding to such interlopers were identified. The oscillations in the calculated predissociation widths for $^1\Sigma_u^+$ are shown to relate to strong nonadiabatic couplings at short internuclear distance and a periodic bias of the wave function toward short distances. This is in accordance with other theory and experiment for ungerade states in molecular hydrogen [21,22]. Within the present framework of dissociation-only nonadiabatic dynamics, it would be interesting to examine the effect of the nonhomogenous coupling for $J > 0$, in particular to $^1\Pi_u$ electronic states.

The present treatment does not include coupling to the ionization and the electronic Rydberg continua and there is significant structure in the experimentally observed levels that is not reproduced. It is hence possible that some of the peaks in the experiment could belong to electronic Rydberg levels corresponding to $v^+ = 5$–8, $N = 2$ series [24]. Questions regarding the interplay of electronic and heavy Rydberg series, the intensities and line shapes, and perhaps most importantly the actual excitation mechanism with which these states are populated, since the direct Franck-Condon factors are small [7], remain open, awaiting a full treatment that combines both ionization and dissociation.

ACKNOWLEDGMENTS

The authors gratefully acknowledge helpful discussions with Elizabeth McCormack, Michèle Glass-Maujean, and Wim Ubachs. A.K. was supported by the European Union through Grant No. COCOSPEC (FP7-IEF) and Ch.J. was supported by ANR (France) under Contract No. 09-BLAN-020901.

[1] A. Suits and J. W. Hepburn, Annu. Rev. Phys. Chem. **57**, 431 (2006).
[2] X. Liu, R. L. Gross, and A. G. Suits, Science **294**, 2527 (2001).
[3] S. C. Glover, D. W. Savin, and A.-K. Jappsen, Astrophys. J. **640**, 553 (2006).
[4] M. Stenrup, Å. Larson, and N. Elander, Phys. Rev. A **79**, 012713 (2009).
[5] T. Ross, E. J. Baker, T. P. Snow, J. D. Destree, B. L. Rachford, M. M. Drosback, and A. G. Jensen, Astrophys. J. **684**, 358 (2008).
[6] M. O. Vieitez, T. I. Ivanov, E. Reinhold, C. A. de Lange, and W. Ubachs, Phys. Rev. Lett. **101**, 163001 (2008).
[7] M. O. Vieitez, T. I. Ivanov, E. Reinhold, C. A. de Lange, and W. Ubachs, J. Phys. Chem. A **113**, 13237 (2009).
[8] R. C. Ekey Jr. and E. F. McCormack, Phys. Rev. A **84**, 020501 (2011).
[9] S. Mollet and F. Merkt, Phys. Rev. A **82**, 032510 (2010).
[10] A. Kirrander, J. Chem. Phys. **133**, 121103 (2010).
[11] G. Staszewska and L. Wolniewicz, J. Mol. Spectrosc. **212**, 208 (2002).
[12] L. Wolniewicz, T. Orlikowski, and G. Staszewska, J. Mol. Spectrosc. **238**, 118 (2006).
[13] P. Quadrelli, K. Dressler, and L. Wolniewicz, J. Chem. Phys. **92**, 7461 (1990).
[14] D. E. Manolopoulos, J. Chem. Phys. **85**, 6425 (1986).
[15] L. Wolniewicz, J. Chem. Phys. **108**, 1499 (1998).
[16] C. L. Pekeris, Phys. Rev. **126**, 1470 (1962).
[17] A. Dalgarno, Adv. Phys. **11**, 281 (1962).
[18] J. M. Hutson, Comput. Phys. Commun. **84**, 1 (1994).
[19] Ch. Jungen and F. Texier, J. Phys. B **33**, 2495 (2000).
[20] E. F. McCormack (private communication).
[21] M. Glass-Maujean, S. Klumpp, L. Werner, A. Ehresmann, and H. Schmoranzer, J. Phys. B **40**, 19 (2007).
[22] R. Lefebvre, Chem. Phys. Lett. **451**, 14 (2008).
[23] M. Glass-Maujean, Ch. Jungen, H. Schmoranzer, I. Haar, A. Knie, P. Reiss, and A. Ehresmann, J. Chem. Phys. **135**, 144302 (2011).
[24] D. Sprecher (private communication).